Research Square

Preprints are preliminary reports that have not undergone peer review.
They should not be considered conclusive, used to inform clinical practice,
or referenced by the media as validated information.

Contactless Medical Equipment AI Big Data Risk Control and Quasi Thinking Iterative Planning

zhu rongrong (rongrongzhu1969@163.com)
Fudan University

Article

Keywords: AI data risk control, Quasi thinking iterative planning, Heavy core clustering tanh equilibrium, Heavy core clustering lens, RBF complex variable feature space kernel

Posted Date: December 1st, 2021

DOI: https://doi.org/10.21203/rs.3.rs-1100366/v1

License: This work is licensed under a Creative Commons Attribution 4.0 International License.
Read Full License

Contactless Medical Equipment AI Big Data Risk Control and Quasi Thinking Iterative Planning

Zhu Rongrong, Fudan University, Shanghai, China

rongrongzhu1969@163.com

ABSTRACT

Contactless medical equipment AI big data risk control and quasi thinking iterative planning，The tanh equilibrium state of heavy core clustering based on hierarchical fuzzy clustering system based on differential incremental equilibrium theory is adopted. Successfully control the parameter group of CT / MR machine internal data, big data AI mathematical model risk. The polar graph of high-dimensional heavy core clustering processing data is regular and scientific. Compared with the discrete characteristics of the polar graph of the original data. So as to correctly detect and control the dynamic change process of CT / MR in the whole life cycle. It provides help for the predictive maintenance of early pre inspection and orderly maintenance of the medical system. It also puts forward and designs the big data depth statistics of AI risk control medical equipment, and establishes the standardized model software. Scientifically evaluated the exposure time and heat capacity MHU% of CT tubes, as well as the internal law of MR (nuclear magnetic resonance), and processed big data twice and three times in heavy nuclear clustering. After optimizing the algorithm, hundreds of thousands of nonlinear random vibrations are carried out in the operation and maintenance database every second, and at least 30 concurrent operations are formed, which greatly improves and shortens the operation time. Finally, after adding micro vibration quasi thinking iterative planning to the uncertain structure of AI operation, we can successfully obtain the scientific and correct results required by high-dimensional information and images. This kind of AI big data risk control improves the intelligent management ability of medical institutions, establishes the software for predictable maintenance of AI big data, which is cross platform and embedded into the web system.

Keywords: AI data risk control,Quasi thinking iterative planning, Heavy core clustering tanh equilibrium, Heavy core clustering lens, RBF complex variable feature space kernel

* Fudan University, Shanghai, China
rongrongzhu1969@163.com

1 INTRODUCTION

The tanh equilibrium of heavy core clustering is based on the hierarchical fuzzy clustering system based on differential incremental equilibrium theory. Cross platform language development and web integrated design and deployment of big data AI mathematical model risk control for internal information of large medical equipment. It provides a decision analysis system for hospital intelligent management. Through the 3D polar coordinate system image analysis of high-dimensional traceability system for the heavy core clustering processing data of big data. At the same time, the software system carries the monitoring of abnormal data of risk control and successfully traces back to the original data. At the same time, the correctness and scientificity of AI mathematical model risk control have been partially verified. Because the system will also make AI image comparison and deep learning for these abnormal data to judge whether there is a false positive. The cross platform big data development platform will successfully establish AI 3d mathematical model scientific computing and image display, and form image cognition and matching. Because of the mathematical innovation of artificial intelligence, the complexity of AI software system design and the pressure brought by its software performance and huge multi process concurrent operation are greatly reduced. Non contact medical equipment AI big data risk control and quasi thinking iterative planning successfully solved the mathematical model unification and standardization of risk control of different equipment, and automatically adjusted its core parameter group to form different boundary threshold distribution. In this way, it is very easy to analyze the comprehensive evaluation index domain of reliability between different CT / MR and the same equipment type.

1.1 Mathematical model core formula of artificial intelligence big data advanced risk control and quasi thinking iterative planning

$$P^{(1)}_{(A_i\ ,A_j)} = \left(\frac{1}{4}\right)^n \left[Sin\left(A_1 + \sum_{i=2}^{m} A + n\cdot\frac{\pi}{4}\right) + Sin\left(A_1 - \sum_{i=2}^{m} A + n\cdot\frac{\pi}{4}\right)\right]^{n-1}_{P^*_{i(x,y)}} \quad (1)$$

$$P^{(2)}_{(A,\ B)} = \left(\frac{1}{4}\right)^{n-1}\sqrt{2}\left[Sin\left(\frac{A_1}{2}+\frac{\pi}{4}+n\cdot\frac{\pi}{4}\right)Cos\left(\sum_{i=2}^{m} A_i + \sum_{i=1}^{m} i\cdot\frac{A_i}{2}\right) - Sin\left(\frac{B_1}{2}+\frac{\pi}{4}+n\cdot\frac{\pi}{4}\right)Cos\left(\sum_{i=2}^{m} B_i + \sum_{i=1}^{m} i\cdot\frac{B_i}{2}\right)\right]^{n-1}_{P^*_{ij}(x_i,y_j)} \quad (2)$$

1.2 The depth statistics kernel is integrated into the quasi normal topological projection conjugate wavelet neural network to improve the big data reliability of the internal parameter group of AI risk control medical equipment

With different parameters, a supersymmetric projection linear narrow-band t → p distribution is formed.

Integrate two cores $t_i = (x_i, y_i), \overline{t_i} = \overline{(x_i, y_i)}$ into $[Tanh \times Ctanh]^{\nabla}$, i.e. $[Tanh(t_i - \overline{t_i}) \times Ctanh(t_i + \overline{t_i})]^{\nabla}$.

Partial normal heavy kernel weight probability density gradient (1,2) - order quasi normal topological stability structure projection conjugate wavelet neural network image reflection risk control p-value distribution is of great significance. The heavy core clustering positive anomaly data group, negative weak anomaly data group and normal data group are separated.

$$[Tan\hbar \times Ctan\hbar]^{\nabla}$$

$$= \frac{\left[\frac{k^2\sigma_1}{\sqrt[3]{\frac{\pi^2}{4}}} \times e_{ij}^{\frac{1}{8}\left[\left(X_i - i\bar{X}\right)_i - \frac{\mu}{\sigma}\right]^3} \theta_{\sqrt{\pi}}^{+2}(X_{ij}X_{i+1,j+1}) - \frac{k^2\sigma_2}{\sqrt[3]{\pi^2}} \times e_{ij}^{-\frac{1}{8}\left[\left(X_i + i\bar{X}\right)_j - \frac{\mu}{\sigma}\right]^3} \theta_{\sqrt{\pi}}^{+2}(X_{i+1,j+1}X_{ij})\right]}{\left[\frac{k^2\sigma_3}{\sqrt[3]{\pi^2}} \times e_{ij}^{\frac{1}{8}\left[\left(X_i - i\bar{X}\right)_i - \frac{\mu}{\sigma}\right]^3} \theta_{\sqrt{\pi}}^{+2}(X_{ij}X_{i+1,j+1}) + \frac{k^2\sigma_4}{\sqrt[3]{\frac{\pi^2}{4}}} \times e_{ij}^{-\frac{1}{8}\left[\left(X_i + i\bar{X}\right)_j - \frac{\mu}{\sigma}\right]^3} \theta_{\sqrt{\pi}}^{+2}(X_{i+1,j+1}X_{ij})\right]}$$

$$\otimes \frac{\left[\frac{k^2\sigma_5}{\sqrt[3]{\pi^2}} \times e_{ij}^{\frac{1}{8}\left[\left(X_i - i\bar{X}\right)_i - \frac{\mu}{\sigma}\right]^3} \theta_{\sqrt{\pi}}^{-2}(X_{ij}X_{i+1,j+1}) + \frac{k^2\sigma_6}{\sqrt[3]{\frac{\pi^2}{4}}} \times e_{ij}^{-\frac{1}{8}\left[\left(X_i + i\bar{X}\right)_j - \frac{\mu}{\sigma}\right]^3} \theta_{\sqrt{\pi}}^{-2}(X_{ij}X_{i+1,j+1})\right]}{\left[\frac{k^2\sigma_7}{\sqrt[3]{\frac{\pi^2}{4}}} \times e_{ij}^{\frac{1}{8}\left[\left(X_i - i\bar{X}\right)_i - \frac{\mu}{\sigma}\right]^3} \theta_{\sqrt{\pi}}^{-2}(X_{ij}X_{i+1,j+1}) - \frac{k^2\sigma_8}{\sqrt[3]{\pi^2}} \times e_{ij}^{-\frac{1}{8}\left[\left(X_i + i\bar{X}\right)_j - \frac{\mu}{\sigma}\right]^3} \theta_{\sqrt{\pi}}^{-2}(X_{ij}X_{i+1,j+1})\right]}$$

$$, and\ \sigma\left(\pi, \frac{\pi}{4}, \frac{\pi}{2}, 2\pi\right)^{-T^2} \to \sigma\left(\pi, \frac{\pi}{4}, \frac{\pi}{2}, 2\pi\right)^{T^2} \text{, form a high-dimensional information field} \quad (3)$$

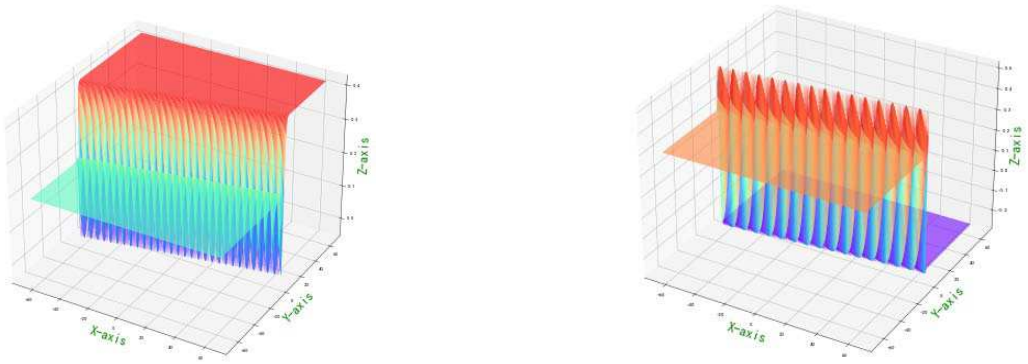

Figure 1: Partial normal heavy kernel weight probability density gradient (1,2) - quasi normal topological stability structure projection conjugate wavelet neural network image reflection risk control p-value image.

2 COMPARATIVE ANALYSIS OF EXPOSURE TIME AND HEAT CAPACITY MHU% OF CT TUBES

The quasi thinking iterative planning of heavy core clustering tanh equilibrium structure in the risk control of ICT 256 equipment finds a special stable AI standard calculation model.

The hierarchical fuzzy clustering system based on differential incremental balance theory is fused with tanh partial normal, and the vibration parameters are inserted into the parameter group. The above processing data of risk control are used for KNN neural network learning and training. For example, KNN is used to obtain the reliability learning form of the adjacent domain, successfully capture the abnormal phenomena of the original data, and judge whether it is false positive through AI mathematical model risk control model. High dimensional data model of CT actual processing data (heavy core clustering tanh). From this, the stability of ICT 256 equipment can be analyzed, and its reliability percentage is 89.801% to 92.419%. Its image is as follows.

2.1 The quasi thinking iterative planning of heavy core clustering tanh equilibrium structure in the risk control of ICT 256 equipment finds a special stable AI standard Computation model

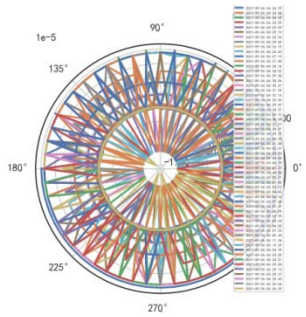

Figure 2: CT tubes exposure time big data heavy core clustering image.

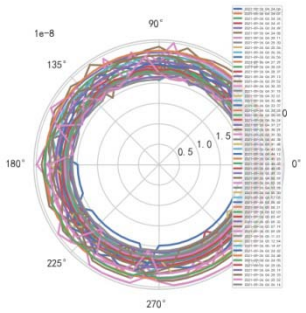

Figure 3: CT heat capacity MHU% big data heavy core clustering image.

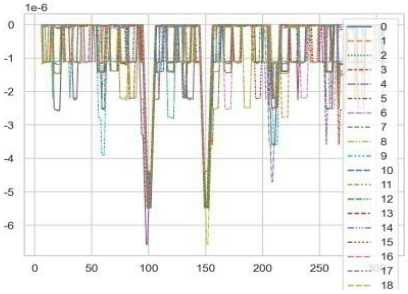

Figure 4: CT tubes exposure time big data additive heavy core cluster image.

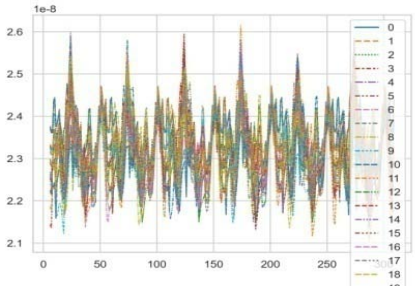

Figure 5: CT heat capacity MHU% big data additive heavy core cluster image.

Compared with the discrete characteristics of the polar graph of the original data, the following image.

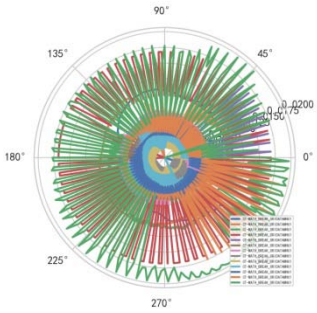

Figure 6: Original data analysis model of CT tubes exposure time.

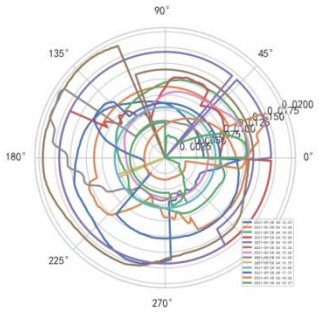

Figure7: Original data analysis model of CT tubes exposure time.

2.2 Similarly,it can be found that the exposure time and heat capacity MHU% of CT tubes show unstable AI mathematical model risk control

When the quasi thinking iterative planning of heavy core clustering tanh equilibrium structure in SERIALNO CT equipment risk control, a special stable AI non-standard Computation model is found, and it cannot judge the reliability of equipment risk control. Therefore, considering the signal fluctuation parameter group of transformation quasi thinking, AI dynamic adjustment and N iterations to obtain its AI standard Computation model. If the appropriate pseudo thinking heavy core clustering AI mathematical model risk control SERIALNO CT with tanh equilibrium structure, the stability and reliability percentage of its normal ball pipe is > 80% and < 99%. If there are inappropriate quasi thinking iterative programming. The AI risk control of its heavy core clustering tanh equilibrium secondary processing data is less than 67.348%, so it needs AI re iteration.

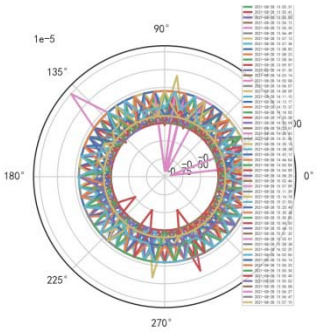

Figure8: Big data analysis model of exposure time of CT tubes.

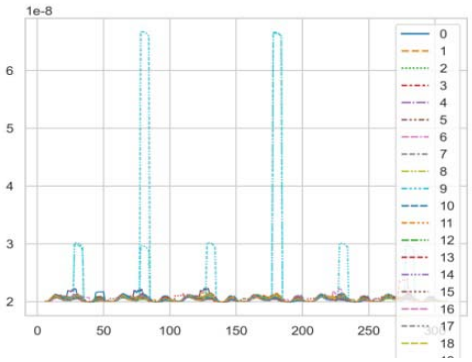

Figure9: CT heat capacity MHU% big data analysis model.

2.3 The significance of establishing a new generation of medical AI big data platform [heavy core clustering quasi thinking iterative planning]

Capture the most important quasi thinking wave curve (signal), iterate and determine the condition, namely domain value, through the vibration of random function and AI operation. If possible, the fluctuation curve of human (thinking) brain wave signal, that is, the iterative evolution of brain like AI form on the reliability of risk control of the above large medical equipment from weak to strong, can be used to provide a basis for obtaining risk control of CT large equipment.The reliability percentage data of risk control of large medical equipment are analyzed by long-time distribution curve. It can be learned and trained by KNN of AI neural network. Moreover, the heavy core data corresponding to this reliability < + [1,10] - [1,10] > is KNN of dual core neural network, and the correct risk control successful data are marked through unsupervised learning.

3 RISK CONTROL OF UNSTABLE AI DATA FOR SERIALNO_CT TUBES EXPOSURE TIME AND HEAT CAPACITY

The SERIALNO_CT is calculated twice (with random vibration function and data vibration), and then the differential difference calculation is carried out by the second set of formula of

hierarchical fuzzy clustering system based on differential incremental balance theory through big data to form a standard calculation model.

How to build a reasonable AI risk control model through multiple iterations of big data heavy core clustering. The ultra flat structure of weakened heavy core clustering data (SERIALNO_CT) is magnified slightly, so that the small fluctuating heavy core has lens amplification effect.

3.1 Transform the quasi thinking signal fluctuation parameter group, AI dynamic adjustment and N iterations to obtain the standard Computation model

$$\frac{\text{Weakened heavy nuclear tanh equilibrium}}{\text{SERIALNO\_CT}} \xrightarrow{\text{Heavy nuclear lens}} \frac{\text{Strengthened heavy nuclear tanh equilibrium}}{iCT256}$$

Tanh equilibrium state of super flat weakened heavy nucleus $\xrightarrow{\text{Heavy nuclear lens}}$ The tanh equilibrium of non super flat enhanced heavy nuclei, while the second set of formulas has the ability to analyze data in a higher dimension (high lens effect).

3.2 How to transform the above design into AI programming system

The 2-day SERIALNO_CT heavy core data can be processed by high lens effect, that is, the second set of formulas for heavy core clustering. How to obtain 2 batches of heavy core clustering data of SERIALNO_CT and how to trace the original data.

How to determine the adjacent data with reliability boundary (threshold) < 67.3349%. The high lens data distribution is constructed. After two batches of data AI operations, the non ultra flat enhanced heavy core tanh equilibrium is formed, and the data storage table of non ultra flat enhanced (high lens) heavy core tanh equilibrium is generated. Image KNN_AI programming process, generate heavy core clustering image, form CT tubes exposure time, and heat capacity MHU% analysis model. And form a [1,10] heavy core clustering table, which can compute the percentage of reliability through the above programming process, store it in the [1,10] clustering table, and finally send it to the image database for KNN display, and embed the web for HTML display. There are two [10,10] high lens clustering data processing for 3 times in the ultra flat weakened heavy core tanh equilibrium.

4 COMPARE THE PROPERTIES, DUCTILITY, FUNCTIONAL COMPREHENSIVENESS, RELIABILITY, ETC. OF ICT256 AND UCT528

Clustering tanh equilibrium from heavy nuclei strengthens the heavy nucleus tanh equilibrium. It can be seen that iCT256 is a high-end CT with superior performance, a wide range of check body parts and rich parameters of machine motion state; It is very consistent with the standard algorithm model of quasi thinking iterative programming for heavy core clustering. Therefore, the risk control of big data AI mathematical model has carried out long-term tracking unsupervised learning from ict256. Therefore, iCT256 has a higher price for a single machine, so it is of greater significance to use AI mathematical model risk control.

4.1 The overall evaluation of iCT256 is about 85% (avg), while the overall evaluation of uCT528 is between 55% - 58% (avg)

The extendability of iCT256 performance, it can check more parts of the human body, and can better find out whether there are tissue abnormalities in the patient's body; The results of AI mathematical model risk control also reflect this. Through blind measurement, it can also be correctly found that high-end CT is the highlight of this risk control; The highest comprehensive evaluation reliability ict256 of AI big data mathematical model risk control is [80.264%, 92.937%].

4.2 When the comprehensive reliability of AI mathematical model risk control of iCT256 is more than 80%, it can be basically determined that the newer CT machine is running

When the comprehensive performance reliability of the groups of iCT256 is more than 90%, the absolute standard type of exposure time and CT heat capacity MHU% appears, which is very scientific. When big data reaches a certain degree, it can completely distinguish the old and new models and service time of iCT256, so it plays a key role in predicting CT life. When the above new and old iCT256 groups determine the life risk control, and through KNN neural network training, the prediction of CT life reaches very high accuracy, so the risk control of large medical equipment in the hospital is of great significance. AI deep polymorphic overlay mathematical model risk control can be carried out for iCT256 and uCT528, which can clearly distinguish their comprehensive performance. The average value of the former is > 80%, and the range of the latter is 55% - 58%. Through the above AI big data mathematical model risk control, it can provide an important parameter group for uct528 to improve the performance of CT equipment, so that its CT innovation can reach the ranks of high-end CT with good ductility, multi-function, high performance and high reliability, and has a core competitive advantage with iCT256.

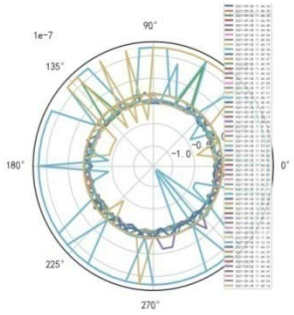

Figure10: uCT528 exposure time [comprehensive reliability 57.45%].

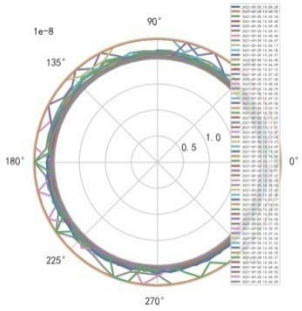

Figure11: uCT528 heat capacity MHU% [comprehensive reliability 57.45%].

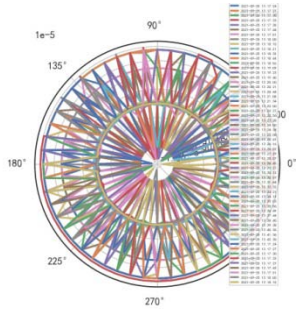

Figure12: iCT256 exposure time [comprehensive reliability 92.937%].

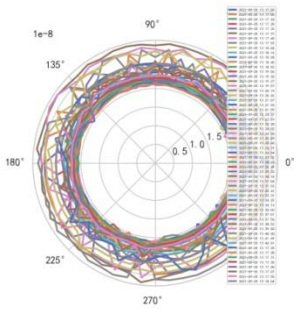

Figure13: iCT256 heat capacity MHU% [comprehensive reliability 92.937%].

5 MRI IMAGE DEFINITION, PEAK SAR RF AI MATHEMATICAL MODEL RISK CONTROL

Assume $\delta = center\_frequency/imageing\_frequency$, $\omega = (TR \otimes TE)$, MR=Image Definition

$$MR = \frac{\boldsymbol{\delta}}{\omega} Matrix \begin{bmatrix} excitions\_number & & \\ & spacing\_between\_slices & \\ & & magnet\_field\_strength \end{bmatrix}$$

Image definition formula, diagonal matrix signal transmission and reception form. Therefore, to some extent, sometimes its magnetic resonance signal can be received and interpreted.

$$MR^{(x,y,z)}_{Image\_Definite} = \frac{\delta}{\omega} \times Matrix \begin{bmatrix} E_x & & \\ & S_y & \\ & & m_z \end{bmatrix}$$

The general formula of MRI image definition is as follows:

$$\underset{Def.}{^{Image}}\mathrm{MR}^{H_{ij}\,Q_i H_{ji}^H}_{More\_patients} =$$

$$\sum_{i=1}^{k} \frac{\boldsymbol{\delta}}{\omega_i} \times log \left| I + R^{-1} \times H_{ij} \times Matrix \begin{bmatrix} E_x & & \\ & S_y & \\ & & m_z \end{bmatrix}_i^Q \times H_{ji}^H \right|, and\ R^{-1}\ \ interference\ signal,$$

$$E_x = excitions\_number, S_y = spacing\_between\_slices, m_z = magnet\_field\_strength,$$

$$\omega_i = (TR \otimes TE) \qquad (4)$$

Therefore, the image definition of MR is directly related to the interference signal (R^{-1}). It is also related to the performance of MR machine, that is, whether it is high-end MR.

The image of high-dimensional signal (information polar coordinates) of MR DISCOVERY MR750w is as follows:

Figure14: MR image definition heavy core clustering tanh balanced big data risk control high-dimensional data polar coordinates graph.

$\omega_i = (TR \otimes TE)$ is a constraint parameter. $1/\omega_i$ controls the stability morphological characteristics of high-dimensional information distribution

$$Q_{MR}^{core\ ener\ gy} = Matrix\begin{bmatrix} E_{X_E}^k \otimes X_k^H & & \\ & E_{X_S}^k \otimes X_k^H & \\ & & E_{X_M}^k \otimes X_k^H \end{bmatrix}_i^Q, E_{X_E}^k \otimes X_k^H, E_{X_S}^k \otimes X_k^H \text{ Sub core energy structure} \quad (5)$$

boundary, and its image is as above.The core energy and sub core energy structure Q of MR, $Q = E\{X_k X_k^H\}$

The simplified general formula for MR image definition is as follows:

$$\underset{Image\_Definite}{\overset{Image}{\mathrm{MR}}}_{More\_patients}^{H_{ij}\,Q_i\,H_{ji}^H} = \sum_{i=1}^{k} \frac{\boldsymbol{\delta}}{\omega_i} \times log\left|I + R^{-1} \times H_{ij} \times Q_{MR}^{core\ energy} \times H_{ji}^H\right|, and\ R^{-1} \text{ Interference signal} \quad (6)$$

5.1 When the R^{-1} interference signal is strengthened, the clarity of MR image decreases and the comprehensive evaluation index decreases

The MR parameter is related to the machine parameter ω = (TR ⊗ TE),excitions_number, spacing_between_slices, magnet_field_strength,SAR

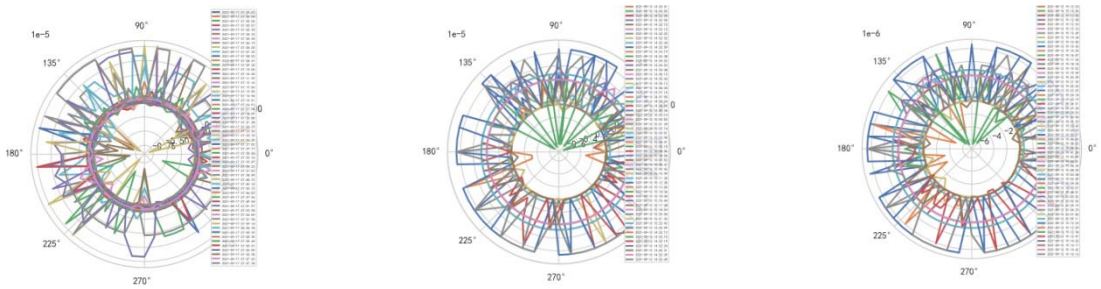

Figure15: MR image definition and performance were 54.398%, 41.551% and 45.473% respectively.

Comprehensive evaluation indexes: 54.398%, 41.551%, 45.473%; Its core boundary is 40.01%, and the scientificity of the image is reduced.

5.2 When $\mathbf{R^{-1}}$ interference signal decreases, MR image clarity increases and comprehensive evaluation index increases

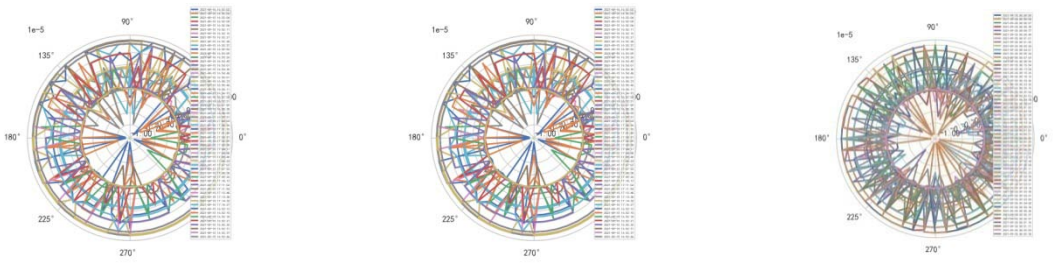

Figure16: MR image definition and performance were 69.730%, 62.940% and74.716% respectively.

Comprehensive evaluation indexes: 69.730%, 62.940%, 74.716%; Its core boundary is 40.01%, and the image is more scientific.

5.3 MR peak SAR RF (similar to CT exposure time high-dimensional data heavy core clustering mathematical model)

if SAR>11.2 then MR stop, When SAR drops down, start MR again. MR does not need to set the domain value, because AI mathematical model risk control can dynamically find the domain value and boundary of various internal indicators of MR machine; This is the advantage of AI system, and adopts the most cutting-edge and advanced original innovative mathematics to combine with AI.Medical equipment management is characterized by high professionalism, high compliance requirements, diverse types and uses, scattered applicable standards and regulations, and large time and space span of equipment management.

AI mathematical model risk control can automatically and dynamically find the domain values and boundaries of various medical equipment indicators, such as the domain values and boundaries of CT's heat capacity and internal indicators of the machine.

Figure17: Heat capacity machine internal index and domain value of CT [weight kernel clustering tanh equilibrium big data risk control high-dimensional data] polar graph.

AI mathematical model risk control automatically and dynamically finds the index domain values and boundaries of various medical equipment. Such as MR peak SAR RF, image definition, internal index domain value and boundary of the machine.

Figure18: Machine internal index domain value of MR image clarity measurement [weight kernel clustering tanh equilibrium big data risk control high-dimensional data] polar graph.

5.4 Application scenario of tanh equilibrium state of non super flat enhanced heavy nucleus

Analyze the stability of DISCOVERY MR750w equipment. AI mathematical model risk control big data found that the ductility, versatility and high reliability of MR equipment DISCOVERY MR750w are also an important basis for judging whether it is a high-end MR. The reliability boundary is 40.01%, which also reflects another important basis for high-end MR. MR peak SAR RF (heavy core clustering tanh balanced core data is similar to CT exposure time), high-dimensional signal image, and AI mathematical model risk control image similar to CT exposure time.

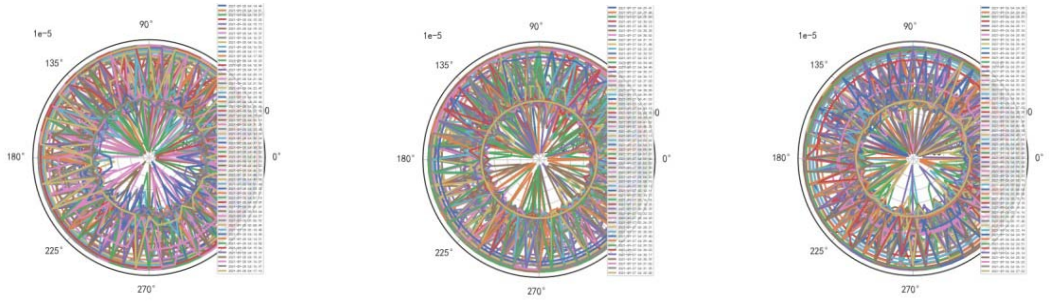

Figure19: MR peak SAR heavy core clustering tanh balanced big data risk control high-dimensional data polar coordinates graph.

6 THE CLUSTERING LENS EFFECT OF TANH EQUILIBRIUM HEAVY CORE OF SUPER FLAT WEAKENED HEAVY CORE AND NON SUPER FLAT ENHANCED HEAVY CORE

6.1 Enhancement of tanh equilibrium lens effect by heavy core hypersphere

The distribution of particles in high dimensions can be observed from the heavy nuclear lens effect on the hypersphere with nuclear magnetic resonance particle energy distribution.

$K=1-\frac{[Ker]}{\frac{(A_i\otimes B_i)_*^{\Delta^2}}{S^2}}+\cdots,[Ker]_{(A_i\otimes B_i)_*^{\Delta^2}}$ is the *s*-1 kernel of the 2-order hypersphere, so the *s*-1-dimensional kernel of the higher-order (2-order) hypersphere $KER_{核}^{P}$ kernel of the complex variable heavy kernel can be derived.

$$KER_P^{i\cdot(Sin,Cos)^2}=\left[Sin^2\left(\sum_{i=2}^{m}A_i+\sum_{i=1}^{m}i\cdot\frac{A_i}{2}\right)+Cos^2\left(\sum_{i=2}^{m}B_i+\sum_{i=1}^{m}i\cdot\frac{B_i}{2}\right)\right]$$

$$\begin{cases}K=1-i\cdot\dfrac{\lambda_i\left[KER_P^{i\cdot(Sin,Cos)^2}\right]^{s-1}}{S^2}-i^2\dfrac{\lambda_{i+1}\left[KER_P^{i\cdot(Sin,Cos)^2}\right]^{s-2}}{S^2}+i^3\cdot\dfrac{\lambda_{i+2}\left[KER_P^{i\cdot(Sin,Cos)^2}\right]^{s-3}}{S^2}-\cdots\\ K=1-\dfrac{\lambda_i\left[KER_P^{i\cdot(Cos,-Sin)^2}\right]^{s-1}}{S^2}-\dfrac{\lambda_{i+1}\left[KER_P^{i\cdot(Cos,-Sin)^2}\right]^{s-2}}{S^2}+\dfrac{\lambda_{i+2}\left[KER_P^{i\cdot(Cos,-Sin)^2}\right]^{s-3}}{S^2}-\cdots\end{cases}\tag{7}$$

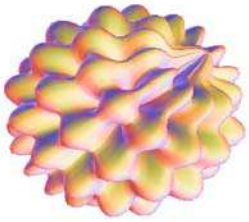

Figure20: The RBF characteristic space of heavy nuclear hypersphere enhancing tanh equilibrium lens effect is the Taylor series expansion of complex variable hypersphere kernel function.

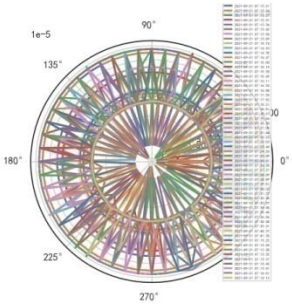

Figure21: CT tubes exposure time big data heavy core clustering high-dimensional information map.

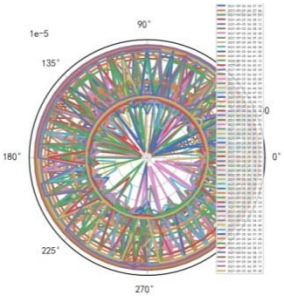

Figure22: MR peak SAR big data heavy core clustering high-dimensional information map.

The super flat structure of the weakened heavy core clustering data is magnified slightly, and the small fluctuation heavy core is constructed, which has the effect of lens amplification.

$$\sum_{j=1}^{m}\sum_{i=1}^{m}\nabla_{ker}\,P_{(2)}^{+}\left(x_i,y_j\right)=\left[\frac{{}_{G}P_{x_i}^{2}}{Cos^{2}\left(\sum_{i=2}^{m}x_i+\sum_{i=1}^{m}i\cdot x_i/2\right)}+\frac{{}_{G}P_{y_j}^{2}}{Sin^{2}\left(\sum_{j=2}^{m}y_j+\sum_{j=1}^{m}j\cdot y_j/2\right)}\right]_{(2)}^{\frac{1}{2}}$$

$$\times\, arctg\left[\frac{Sin\left(\sum_{j=2}^{m}y_j+\sum_{j=1}^{m}j\cdot y_j/2\right)}{Cos\left(\sum_{i=2}^{m}x_i+\sum_{i=1}^{m}i\cdot x_i/2\right)}\right]_{P} \qquad (8)$$

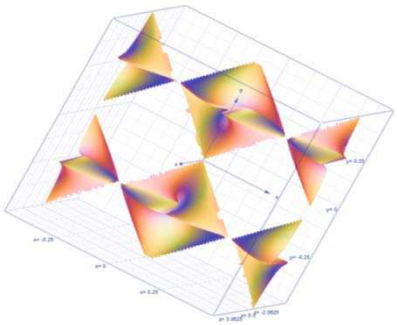

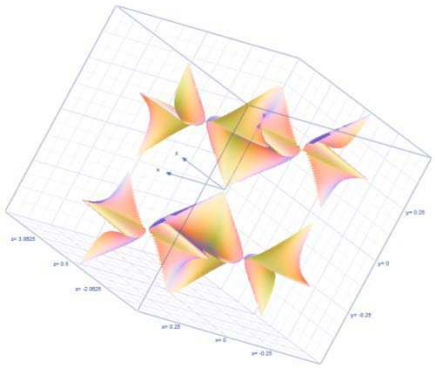

Figure23: Based on the hierarchical fuzzy clustering system based on differential incremental equilibrium theory, the orthogonal subkernel quadratic convolution norm of heavy kernel clustering lens.

$$1 = \left[\frac{{}_{G}P_{x_i}^{2}}{Cos^{2}\left(\sum_{i=2}^{m} x_i + \sum_{i=1}^{m} i \cdot x_i/2\right)} + \frac{{}_{G}P_{y_j}^{2}}{Sin^{2}\left(\sum_{j=2}^{m} y_j + \sum_{j=1}^{m} j \cdot y_j/2\right)}\right]_{(2)}^{\frac{1}{2}} arctg\left[\frac{Sin\left(\sum_{j=2}^{m} y_j + \sum_{j=1}^{m} j \cdot y_j/2\right)}{Cos\left(\sum_{i=2}^{m} x_i + \sum_{i=1}^{m} i \cdot x_i/2\right)}\right]_{P} \quad (9)$$

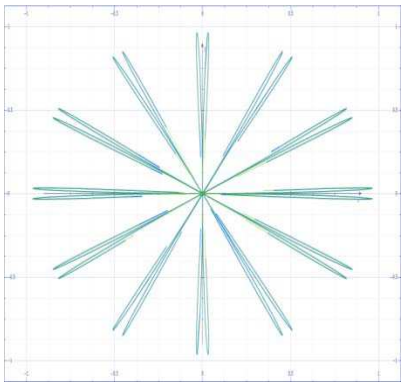

Figure24: Orthogonal subkernel of heavy kernel clustering lens quadratic convolution norm RBF gradient s-dimensional subkernel function -- harmonic function image of topological space.

6.2 The heat capacity weakens the tanh equilibrium state of the heavy core to the series expansion of the restricted RBF hypersphere heavy kernel function

Compute the comparative analysis of the percentage of iCT256 and uCT528 in the comprehensive evaluation of reliability.Through heavy kernel clustering lens orthogonal subkernel quadratic convolution,and form an embedded program. Make the uCT528 approach the high-end iCT256.

According to the analysis of the following formula, the increment index of comprehensive evaluation directly affecting reliability is $arctg\phi(x_i, y_j)$. Therefore, the reliability increment index of uCT528 is controlled between (12.5%, 25%). $if\ \ arctg\left[\frac{Sin\left(\sum_{j=2}^{m} y_j + \sum_{j=1}^{m} i \cdot y_j/2\right)}{Cos\left(\sum_{i=2}^{m} x_i + \sum_{i=1}^{m} i \cdot x_i/2\right)}\right]_{P} \in \left(\frac{\pi}{4}, \frac{\pi}{2}\right)$

$$1 = \left[\frac{{}_{P}G_{x_i}^{2}}{Cos^{2}\left(\sum_{i=2}^{m} x_i + \sum_{i=1}^{m} i \cdot x_i/2\right)} + \frac{{}_{P}G_{y_i}^{2}}{Sin^{2}\left(\sum_{j=2}^{m} y_j + \sum_{j=1}^{m} j \cdot y_j/2\right)}\right]_{(2)}^{\frac{1}{2}} \times arctg\left[\frac{Sin\left(\sum_{j=2}^{m} y_j + \sum_{j=1}^{m} i \cdot y_j/2\right)}{Cos\left(\sum_{i=2}^{m} x_i + \sum_{i=1}^{m} i \cdot x_i/2\right)}\right]_{P} \quad (10)$$

7 CONCLUSION

Contactless medical equipment AI big data risk control and quasi thinking iterative planning. For the first time, this kind of general form is adopted to automatically carry out machine internal information big data AI mathematical model risk control for all large equipment in the hospital,and it has well portabilit. Adding different equipment into the system will automatically detect and display

the information and data of internal operation of the risk control machine. AI big data risk control and quasi thinking iterative planning cross platform web software will be started automatically,and display the risk control data and image display of its whole life cycle. It has a predictable risk control system, that is, a big data intelligent platform for establishing the overall predictability maintenance system of medical institutions.

REFERENCES

[1] Zhu RongRong, Differential Incremental Equilibrium Theory, Fudan University,Vol 1, 2007:1-213

[2] Zhu RongRong, Differential Incremental Equilibrium Theory, Fudan University,Vol 2, 2008:1-352

[3] Liu zhuanghu, Simplicity Set Theory, Beijing China ,Peking University Press，2001.11: 1-310

[4] Xie bangjie, Transfinite Number and Theory of Transfinite Number, Jilin China, jilin people's publishing house,1979.01:1-140

[5] Nan chaoxun , Set Valued Mapping , Anhui China, Anhui University Press , 2003.04: 1-199

[6] Li hongyan, On some Compactness and Separability in Fuzzy Topology, Chengdu China,,Southwest Jiaotong University Press, 2015.06：1-150

[7] Bao zhiqiang , An introduction to Point Set Topology and Algebraic Topology, Beijing China , Peking University Press, 2013.09:1-284

[8] Gao hongya, Zhu yuming , Quasiregular Mapping and A-harmonic Equation, Beijing China , Science Press, 2013.03：1-218

[9] C. Rogers W. K. Schief, Bäcklund and Darboux Transformations: Geometry and Modern Applications in Solition Theory, first published by Cambridge University, 2015: 1-292.

[10] Ding Peizhu,Wang Yi, Group and its Express, Higher Education Press, 1999: 1-468.

[11] Gong Sheng, Harmonic Analysis on Typical Groups Monographs on pure mathematics and Applied Mathematics Number twelfth, Beijing China, Science Press, 1983: 1-314.

[12] Gu chaohao, Hu Hesheng, Zhou Zixiang, DarBoux Transformation in Solition Theory and Its Geometric Applications (The second edition), Shanghai science and technology Press, 1999, 2005: 1-271.

[13] Jari Kaipio Erkki Somersalo, Statistical and Computational Inverse Problems With 102 Figures, Spinger.

[14] Numerical Treatment of Multi-Scale Problems Porceedings of the 13th GAMM-Seminar, Kiel, January 24-26, 1997 Notes on Numerical Fluid Mechanics Volume 70 Edited By WolfGang HackBusch and Gabriel Wittum.

[15] Qiu Chengtong, Sun Licha, Differential Geometry Monographs on pure mathematics and Applied Mathematics Number eighteenth, Beijing China, Science Press, 1988: 1-403.

[16] Ren Fuyao, Complex Analytic Dynamic System, Shanghai China, Fudan University Press, 1996: 1-364.

[17] Su Jingcun, Topology of Manifold, Wuhan China, wuhan university press, 2005: 1-708.

[18] W. Miller, Symmetry Group and Its Application, Beijing China, Science Press, 1981: 1-486.

[19] Wu Chuanxi, Li Guanghan, Submanifold geometry, Beijing China, Science Press, 2002: 1-217.

[20] Xiao Gang, Fibrosis of Algebraic Surfaces, Shanghai China, Shanghai science and technology Press, 1992: 1-180.

[21] Zhang Wenxiu, Qiu Guofang, Uncertain Decision Making Based on Rough Sets, Beijing China, tsinghua university press, 2005: 1-255.

[22] Zheng jianhua, Meromorphic Functional Dynamics System, Beijing China, tsinghua university press, 2006: 1-413.

[23] Zheng Weiwei, Complex Variable Function and Integral Transform, Northwest Industrial University Press, 2011: 1-396.